

Y. Rolland · E. Carrio-Schaffhauser  
S. M. F. Sheppard · A. Pêcher · L. Esclauze

## Metamorphic zoning and geodynamic evolution of an inverted crustal section (Karakorum margin, N Pakistan), evidence for two metamorphic events

Received: 15 September 2003 / Accepted: 27 June 2005  
© Springer-Verlag 2005

**Abstract** The Karakorum Range comprises a crustal section of marbles and metapelites providing an opportunity to study the extent of high-temperature metamorphic reequilibration in an active orogen. Metamorphism culminated during the Mio-Pliocene, at 6–7 Ma. Peak metamorphic conditions increased from south to north, i.e. from (1) the Upper Anchizone grade (lawsonite, chlorite–smectite) to (2) lower granulite migmatite grade (HT~800°C) conditions along strike of a 30-km section perpendicular to the structural fabric of the rocks. The metamorphic section can be separated into two domains:

1. A domain with low to transitional metamorphic conditions, with respect to the HT zone, where initial bedding is preserved. These moderate PT conditions prevailed during the main tectonic stacking event (50–37 Ma), prior to the Mio-Pliocene event. In this domain, metamorphism is governed by fluid-assisted grain-scale diffusion, as suggested by the progressive coarsening of minerals with increasing metamorphic grade and the preservation of sedimentary  $\delta^{13}\text{C}$  signatures in carbonates. A low thermal gradient (17°C/km) is derived from *P-T* estimates of the prograde metamorphic sequences.
2. A higher-grade metamorphic domain where, by contrast, the metamorphic style is dominated by advection of heat with magmatic intrusions involving mantle melts during the recent tectonic history (20–

3 Ma). Strong devolatilisation of  $\text{CO}_2$  and partial melting of the metapelites triggered mixing up of carbonated and pelitic lithologies resulting in ultramafic restites and calc-silicate mobilisates. The  $\delta^{13}\text{C}$  isotopic composition of carbonates is widely modified, though locally preserved.

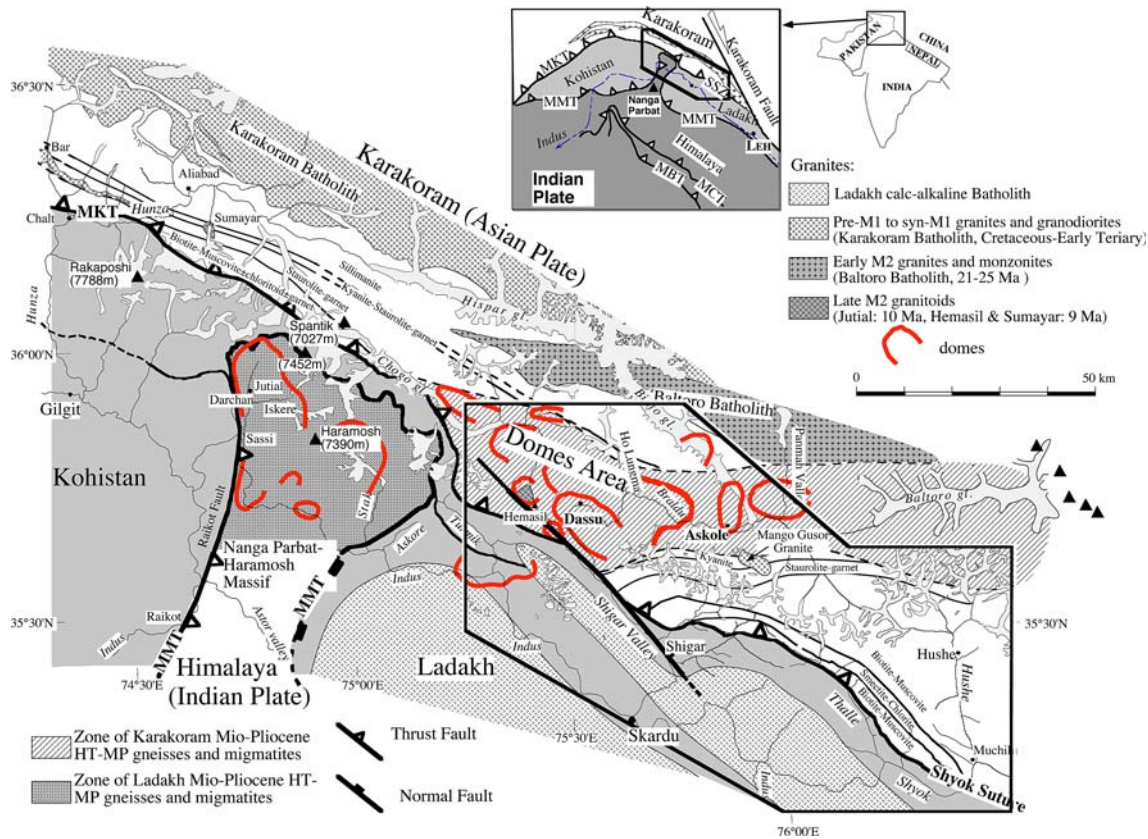
### Introduction

The respective roles of fluid-assisted grain-scale diffusion and magmatic advection in heat and mass transport are widely discussed (Ferry and Gerdes 1998 and references therein). Precise field constraints based on the regional extent of metamorphic equilibration and the nature of percolating fluids are useful to unravel the complex metamorphic history dominated by such processes. The SE Karakorum margin (Fig. 1), or Karakorum Metamorphic Complex (KMC), presents a 20 km thick crustal section, in which the metamorphic conditions of the pelitic series have already been determined on a regional scale, with early Himalayan Barrovian metamorphism culminating at 0.8–1.0 GPa—650–700°C between 55 and 23 Ma, and late high temperature (HT) metamorphism culminating at 0.5–0.6 GPa—750–800°C between 6 and 7 Ma (Bertrand et al. 1988; Hanson 1989; Searle et al. 1989; Allen and Chamberlain 1991; Lemennicier et al. 1996; Rolland et al. 2001). Calc-silicate rocks are also found throughout the KMC metamorphic pile and are more frequent than pelites, especially in the lower-grade part. Previous studies (Bertrand et al. 1988; Searle et al. 1989; Allen et al. 1991; Lemennicier et al. 1996) were mainly concerned with the metamorphism of pelites, so the metamorphic evolution of the lower-grade part remains poorly known. In the calc-silicate lithologies,  $\text{Na}_2\text{O}$  and  $\text{TiO}_2$  contents are low, and the sequence of crystallisation can be described in the K–Ca–(Mg/Fe)–AlSi– $\text{H}_2\text{O}$ – $\text{CO}_2$  system (KCMAS-HC). In this

Y. Rolland (✉)  
Géosciences Azur, 28 Av. Valrose,  
BP 2135, 06108 Nice cédex 2, France  
E-mail: yrolland@unice.fr  
Fax: +04-92-076816

E. Carrio-Schaffhauser · A. Pêcher · L. Esclauze  
LGCA-LGIT, OSUG, Université J. Fourier,  
Maison des Géosciences, BP 53, 38041 Grenoble, France

S. M. F. Sheppard  
UMR 5570, Ecole Normale Supérieure de Lyon,  
Allée d'Italie, 69364 Lyon, France



**Fig. 1** Geological and metamorphic sketch map of the Karakorum margin (NW Himalaya, Pakistan), After Rolland et al. (2001), modified. The **bold frame** is the location of Fig. 3

paper, we report and analyse the successive mineral assemblages occurring with increasing metamorphic grade in calc-silicate rocks of the Karakorum crust. The main objectives are to provide:

1. a crystallisation sequence in the calc-silicate lithology for each step of metamorphism in the crustal section,
2. estimates of  $P-T$  (pressure-temperature) conditions for each assemblage and  $X_{\text{CO}_2}$  values for the  $\text{H}_2\text{O}-\text{CO}_2$  fluid,
3. identification of the metamorphic reactions that responded to changes in  $P-T$ -fluid conditions, using stable isotopic data ( $^{13}\text{C}/^{12}\text{C}$  and  $^{18}\text{O}/^{16}\text{O}$ ) on the rocks for each previously defined metamorphic step.

These data will then be used to reconstruct the geodynamic evolution of the Karakorum inverted crustal section, and help to define the relative roles played by grain-scale diffusion versus magmatic advection of heat.

## Samples and procedures

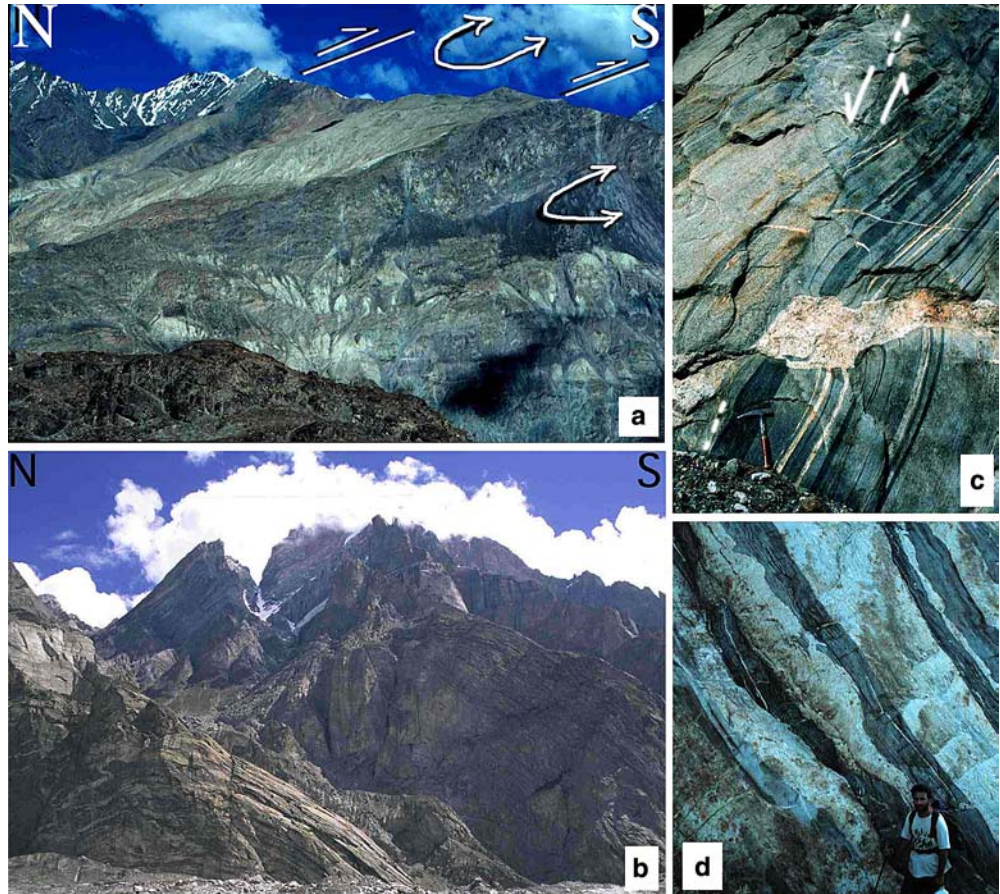
Samples of calc-silicate assemblages come from lower to higher-grade parts of the KMC (Figs. 2, 3). The following procedures have been used on samples:

Mineral identification was done using microscopy and X-ray analyses of selected samples. For X-ray studies, powders were decarbonated in a solution of acetic acid ( $\text{pH} = 5$ ), at  $40^\circ\text{C}$  for 2 days. X-ray diffraction patterns of all samples were recorded on preparations with phyllosilicates oriented by decantation of the  $< 15\text{-}\mu\text{m}$ -size fraction using a Siemens D501 diffractometer at the LGIT of Grenoble. Diffracted-beam monochromatised  $\text{CuK}\alpha$  (1 + 2) radiation was used. Stepping motor drives and intensity acquisition (scintillation detector) were controlled with a Socabim DACO system.

Mineral analyses of selected samples were obtained using a Cameca SX100 electron microprobe at Blaise Pascal University of Clermont-Ferrand. Standards used were natural silicates, with an acceleration voltage of 15 kV and a beam current of 20 nA and a counting time of 10 s per element.

Geochemical analyses were obtained on marbles from the same geological unit (Lower Palaeozoic marbles, see Rolland et al. 2002b). Powders of carbonated rocks were analysed for major and trace elements using both X-ray fluorescence and ICPAES in the LGIT and LGCA of Grenoble. Loss on ignition (LOI) was determined by heating the sample at  $1,000^\circ\text{C}$  for 30 min. Eight marble samples were also selected for stable isotope analyses (for analytical procedures, see Aucour et al. 1999). Analysis of NBS18 standard yielded  $\delta^{13}\text{CPDB} = -5.0\text{‰}$  and  $\delta^{18}\text{OPDB} = -23.0\text{‰}$ . Analytical precision (extraction + spectrometer) was  $\pm 0.05\text{‰}$ .

**Fig. 2** Photographs of the Karakorum Metamorphic Complex. **a** S-verging M1 folds and thrusts along the southern lower-metamorphic grade part of the Karakorum. The picture was taken along the Nubra Valley (India). Marbles are shown up by the white band of rocks in the upper part of the picture. For scale, the height of the face is 2,000 m. **b** M2 metamorphic dome of Panmah (Askole, Pakistan) above the Biafo Glacier. The foliation shape is underlined by migmatitic segregations. For scale, the height of the face is 2,500 m. **c** structural indicators in the Panmah dome core: steep S-dipping ductile shear plane showing a normal offset of horizontal mobilisate veins in a migmatitic gneiss. Horizontal veins indicate a context of horizontal shortening while normal shear planes indicate the extrusion of the dome core relative to its surroundings. **d** ultramafic forsterite-enstatite bearing restites (samples L530-531) and calc-silicated mobilisates (L541) found on the southern slope of the Panmah Dome. Note the difference in structural style between M1 structures (**a**) and M2 structures (**b-d**)



## Geological background

An outline of the geodynamic evolution of the Ladakh–Karakorum area is summarised below. However, for a more detailed synthesis, the reader is referred to Rolland (2002). The main geological features are summarised below.

The core of the Karakorum range is comprised of a large NW–SE elongated composite batholith (the Karakorum Batholith, Fig. 1) formed between 120 and 80 Ma (Debon et al. 1987), related to the subduction of the Tethys ocean along the Shyok Suture Zone and Main Mantle Thrust (Honegger et al. 1982; Rolland et al. 2000, 2002a; Mahéo et al. 2004). The southern margin of the KMC is comprised of Cambro-Ordovician sedimentary series, lying on a Proterozoic crustal basement (Le Fort et al. 1994; Rolland et al. 2002b). The Himalayan metamorphic cycle started with the collision of the Indian and Asian plates at c. 55 Ma (e.g. Rowley 1996 and references therein; de Sigoyer et al. 2000). Still ongoing convergence of these two plates ( $5 \text{ cm year}^{-1}$ ; Patriat and Achache 1984) is accommodated by (1) crustal shortening along NW–SE striking thrusts and folds within the Himalaya and the Karakorum (e.g. Le Fort 1975), with uplift of

more than  $1 \text{ cm year}^{-1}$  locally (e.g. Zeitler et al. 1985), and (2) strike-slip faulting at their periphery (e.g. Tapponnier et al. 1975).

The metamorphic evolution of the Karakorum complex took place in two phases, which are documented from the study of metapelites (Fig. 3a). The first metamorphic phase (M1) corresponds to the thrusting of rocks towards the SW since the onset of the India–Asia collision. This phase is characterised by Barrovian-type metamorphism, with low-grade chlorite-bearing assemblages in the south, and high-grade staurolite + kyanite + almandine garnet  $\pm$  sillimanite in the north (Fig. 3a). M1 culminated at  $600^\circ\text{C}$ – $1.0 \text{ GPa}$ , (Bertrand et al. 1988; Lemennicier et al. 1996; Rolland et al. 2001) with the emplacement of the Baltoro Batholith at 21–25 Ma (U–Pb on zircon, Searle et al. 1989). A second metamorphic phase (M2) has brought up deep crustal rocks to the surface along an E–W crustal-scale fold. The M2 phase is featured by (prismatic) sillimanite + K-feldspar + pyrope-rich garnet and partial melting (Fig. 3a). Within the domes (high-grade zone), the rocks reequilibrated during M2 at  $800^\circ\text{C}$  and  $0.55 \text{ GPa}$  (Rolland et al. 2001). Around the domes (Transition zone), relict M1 assemblages are present and are incompletely transformed into M2 assemblages. This younger M2 event is



et al. 2001). The M2 event is interpreted to result from the intrusion of related mantle-derived magmas (syenites) within the core of the fold, dated at 9 Ma (Villa et al. 1996). The intrusions produced intense migmatization and subsequent doming by diapiric amplification of the anticlinal structure (Rolland et al. 2001; Mahéo et al. 2002).

## Results

### Structure and metamorphic isograds

At the scale of the Karakorum margin, the M1 metamorphic foliation mainly trends NW–SE, parallel to the early Himalayan tectonic contacts such as the Karakorum–Ladakh suture (or Shyok Suture, Fig. 1). M1 metamorphic isograds defined from the occurrence of index minerals in the field and thin sections correspond to jumps in metamorphic grade across south-verging thrusts (Fig. 2a). North of Skardu city, the M1 metamorphic foliation trend becomes more irregular (e.g. Rolland et al. 2001), and reflects reactivation of the foliation in kilometre scale non-cylindrical (roughly conical) folds, which are kilometre-scale domes (Figs. 2b, 1). In the cores of the domes, normal-sense of shear is locally observed (Fig. 2c) and M2 lineations are radial. These tectonic indicators show a context of vertical extrusion of the domes, along an E–W anticlinal axis, that is clearly crosscutting the NW–SE trend of M1 structures (Fig. 1). The domes are also formed by migmatites (Fig. 2c, d) and by the occurrence of higher temperature assemblages M2 sillimanite + K-feldspar (Fig. 3a). Migmatites are characterised by figures of mixing of calcic and pelitic lithologies into migmatites, restites and mobilisates (Fig. 2d).

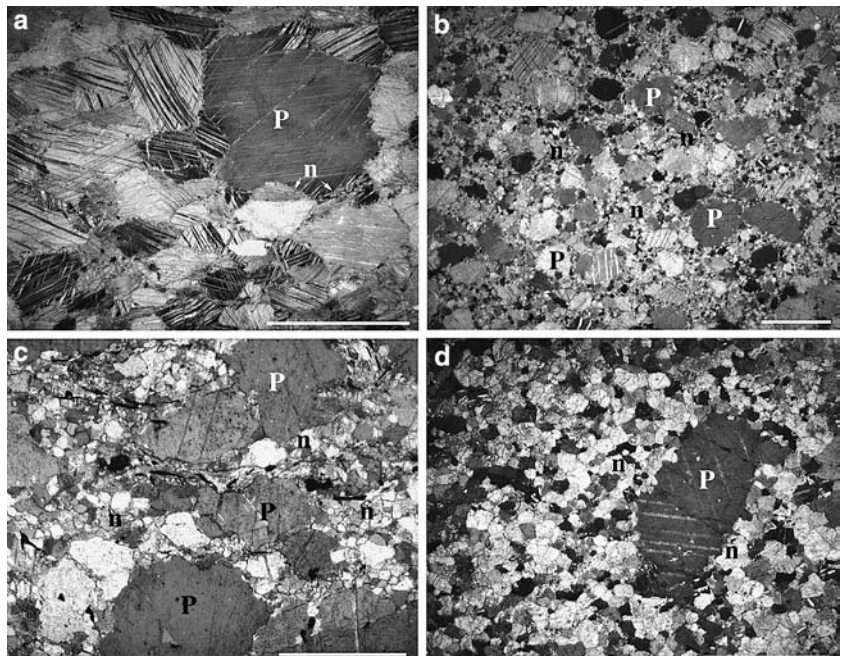
### Regional-scale increase of metamorphic grade

#### *Evolution of textures in calc-silicates with metamorphic grade*

Metamorphism increases progressively on a regional scale (20 km) from low-grade in the south to high-grade in the north (Fig. 3). In the south, M1 metamorphic isograds are parallel to the NW–SE trending foliation and to the main tectonic contacts (as the Shyok Suture Zone). In the north, the high-grade zone (or Dome zone) is bounded by the east–west striking sillimanite-in isograd (M2 event), which cross-cuts the M1 pattern.

In the KMC metamorphic pile, the progressive increase in metamorphic grade is witnessed by the evolution of the geometry of deformation twins (e-twins) in calcite, which has been proposed as a temperature gauge. Lower-grade calcite porphyroclasts (Fig. 4a, b) show narrow straight e-twins that indicate temperatures below 200°C (type I; Bukhard 1993). Minor neoblastic micrometer-large calcite grains occur at the grain boundaries of porphyroclasts (Fig. 4a). Progressive increase of metamorphic grade produced a reorganisation of calcite e-twins evolving to wider twins in porphyroclasts (Fig. 4c), which indicate temperatures between 150 and 300°C (type II-III; Groshong et al. 1984; Rowe and Rutter 1990; Evans and Dunne 1991). The neoblastic grains developed at the expense of porphyroclast grains. At the periphery of the high-grade zone (transition zone), the porphyroclasts are nearly consumed by growth of neoblasts (Fig. 4d). Porphyroclast relics show e-twins with serrated boundaries, defined as type IV twins (>250°C; Vernon 1981; Bukhard 1993).

**Fig. 4** Microphotographs of calcite textures observed with increasing metamorphic grade (a–d) in the marbles. Scale is indicated by the size of *white bars* (250 µm). Sample numbers: **a** L77; **b** L160; **c** L6; **d** L511. *P* porphyroclast, *n* neoblast



The sequence of mineral assemblages in the calc-silicate rocks from the lowest to the highest metamorphic grade is (Table 1):

1. In the Cambro-Ordovician fossiliferous marble lithology (Upper Thalle area, Fig. 3), the lower-grade assemblage (sample L87) is defined by: lawsonite–chlorite–calcite ± smectite ± clinozoisite (1 in Fig. 5; Fig. 6).
2. Further north, the following assemblages occur with increasing metamorphic grade: (sample L82) phengite–chlorite–tourmaline–calcite–clinozoisite–albite (2 in Fig. 5; Fig. 6), (sample L73) phengite–chlorite–tourmaline–calcite–pumpellyite (3 in Fig. 5; Fig. 6), (sample L75) chlorite–phengite–calcite (5 in Fig. 5).
3. North of this lower metamorphic grade area, assemblages without chlorite are observed. (sample L76) muscovite–ankerite–calcite (5 in Fig. 5; Fig. 6), and (sample L77) phengite/muscovite–pyrite–calcite (6 in Fig. 5).
4. To the west, and structurally above this chlorite-free zone, phlogopite-bearing assemblages are observed: (sample L160, Bauma Harel) dolomite–Mg–calcite–muscovite/phlogopite–pyrite–rutile (7 in Fig. 5).
5. In the transition zone, at the periphery of the domes, tremolite-bearing assemblages are observed: (sample L6, Masherbrum and L511, Askole) phlogopite–calcite–Mg–calcite–tremolite–talc (8–9 in Fig. 5; Fig. 6).
6. Finally, in the domes of the Askole area, intense migmatization and lower granulite facies metamorphism have occurred (Fig. 2c,d). Leucocratic 0.5–50 m large bands of calc-silicate composition, comprising the assemblage (sample L541) garnet–plagioclase–quartz–titanite–scapolite–biotite–graphite (11 in Fig. 5; Fig. 6). The calc-silicate pods are formed by the interaction of migmatitic marls produced in metapelites with the neighbouring marble layers (Fig. 2d). The calc-silicate pods comprise ultramafic boudins with the assemblage: (sample L530 and L563) olivine–orthopyroxene–spinel–Mg–chlorite ± magnesite ± talc (10 in Fig. 5; Fig. 6).

**Calcite** In assemblages 1 to 6 (Table 1), calcite is nearly pure with MgO below detection limit and Fe < 0.01 p.f.u. (Table 2). In assemblage 5, it coexists with pure ankerite. In assemblages 7 to 9, Mg–calcite is always present, coexisting with dolomite in assemblage 7, with pure calcite in assemblage 8, and is the only carbonate in assemblage 9.

**Chlorite** In assemblages 1 to 4, chlorite shows a progressive increase in Si (p.f.u.) and correlative decrease in Al (p.f.u.) and  $X_{Fe}$  (Fe/(Fe + Mg)), with correlation coefficients  $R^2$  of 0.6 for the Si versus  $X_{Fe}$  plot and 0.8 for the Al versus  $X_{Fe}$  plot (Fig. 7a). Low Si (p.f.u.) values in the range 5.2–5.5 are obtained for assemblage 1, increasing to 5.7–5.8 in assemblage 4. Al (p.f.u.) values range between 6.0–5.7 in assemblage 1 decreasing and 4.7–4.8 in assemblage 4 (Table 2). Finally, Fe content in chlorites decreases from 4.5–5 p.f.u. in assemblage 1 to 1.4–2 p.f.u. in assemblage 4 (Fig. 7).

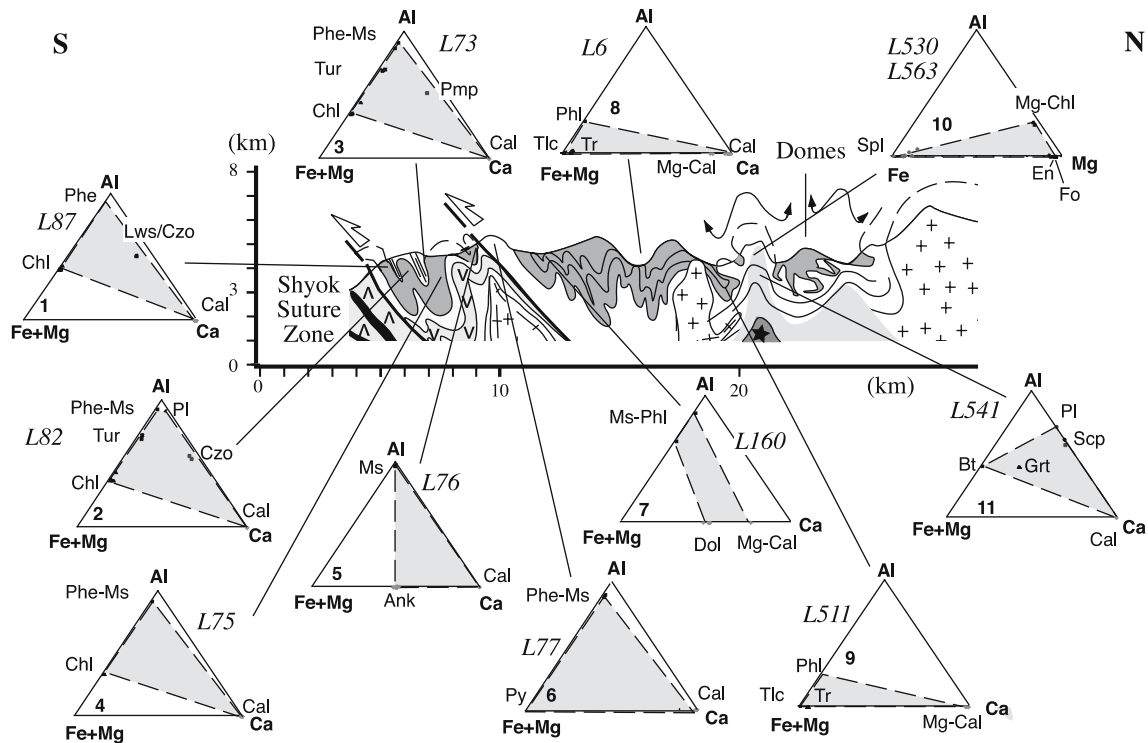
**White micas** From assemblage 2 to 4, a progressive change in composition from muscovite to phengite is observed (Fig. 7b,c). Phengitic micas show a negative correlation ( $R^2=0.6$ ; Fig. 7b) of  $X_{Fe}$  versus Si (p.f.u.). The low  $X_{Fe}$  value of assemblage 5 may be due to contrasting whole-rock composition as emphasised by the presence of ankerite, and will be discussed in the following geochemistry section.

In assemblages 6–7, white mica compositions range between a Mg-rich muscovite (MgO = 0.3–0.4 p.f.u.) to a Mg-poor phlogopite (MgO = 1.8–2 p.f.u.). These compositions suggest mixed layer stacking of both phlogopite and muscovite. In the assemblages 8 and 9, only pure phlogopite ( $X_{Mg} = 2.9–3$  p.f.u.) is observed, which is in agreement with a complete replacement of muscovite by phlogopite.

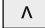

**Lawsonite–pumpellyite–clinozoisite–tourmaline** In assemblage 1, lawsonite is not pure and contains Mg + Fe in substitution to Ca,  $X_{Fe}$  ratio is low (0.3–0.4), while pumpellyite (assemblage 3) is Fe-rich ( $X_{Fe} = 0.9$ ). In assemblages 1 and 2, epidote is a clinozoisite, with high  $Al_2O_3$  contents (30–31 wt%), and relatively low  $Fe_2O_3$

**Table 1** List of studied samples with their mineral assemblages and metamorphic generation (M1/M2)

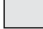

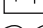


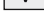
Sample	Assemblage N°	Mineral assemblage
L87	1 (M1)	Lawsonite–chlorite–calcite ± smectite ± clinozoisite
L82	2 (M1)	Phengite–chlorite–tourmaline–calcite–clinozoisite–albite
L73	3 (M1)	Phengite–chlorite–tourmaline–calcite–pumpellyite
L75	4 (M1)	Chlorite–phengite–calcite
L76	5 (M1)	Muscovite–ankerite–calcite
L77	6 (M1)	Phengite/muscovite–pyrite–calcite
L160	7 (M1)	Dolomite–Mg–calcite–muscovite/phlogopite–pyrite–rutile
L6	8 (M1-2)	Phlogopite–calcite–Mg–calcite–tremolite–talc
L511	9 (M1-2)	Phlogopite–Mg–calcite–tremolite–talc
L530 and L563	10 (M2)	Olivine–orthopyroxene–spinel–Mg–chlorite ± magnesite ± talc
L541	11 (M2)	Garnet–plagioclase–quartz–titanite–scapolite–biotite–graphite



### Ladakh :

-  Ladakh terrane (arc and back-arc series) (110-90 Ma)
-  Serpentinized ultramafites

### Karakorum :

-  Granulites (20-5 Ma)
-  Hemasil-type syenite (9 Ma)
-  Granite (37-21 Ma)
-  Limestones
-  Pelites
-  Metavolcanic rocks
- Lower Paleozoic series (Cambrian-Ordovician)

**Fig. 5** Successive assemblages observed with increasing metamorphic grade in marbles of the Lower Paleozoic series along a N-S geological cross-section, from the Shyok Suture Zone (south) to the core of the Karakorum terrain (north). Ternary projections of mineral compositions (*small dots*) are done with mineral compositions in cation% with respect to Al, Fe+Mg and Ca. Mineral abbreviations are following Kretz (1983)

contents (4.6 wt%). In assemblages 1 and 2, tourmalines have  $X_{Fe}$  values of 0.37–0.48.

**Amphibole** Amphiboles, from assemblages 8 and 9, are close to the tremolite end-member (according to Leake et al. 1997), with a very small compositional range (Si p.f.u. varying between 7.9 and 8,  $X_{Fe} \sim 0$  for all samples).

**Talc** Talc compositions are also very homogeneous in these two assemblages with structural formulae  $Si_{8.6-8.8} Al_{0.0-0.1} Mg_{6.4-6.5}$ .

**Orthopyroxene-olivine-Mg-chlorite-spinel** In assemblage 10, all mineral phases show small compositional

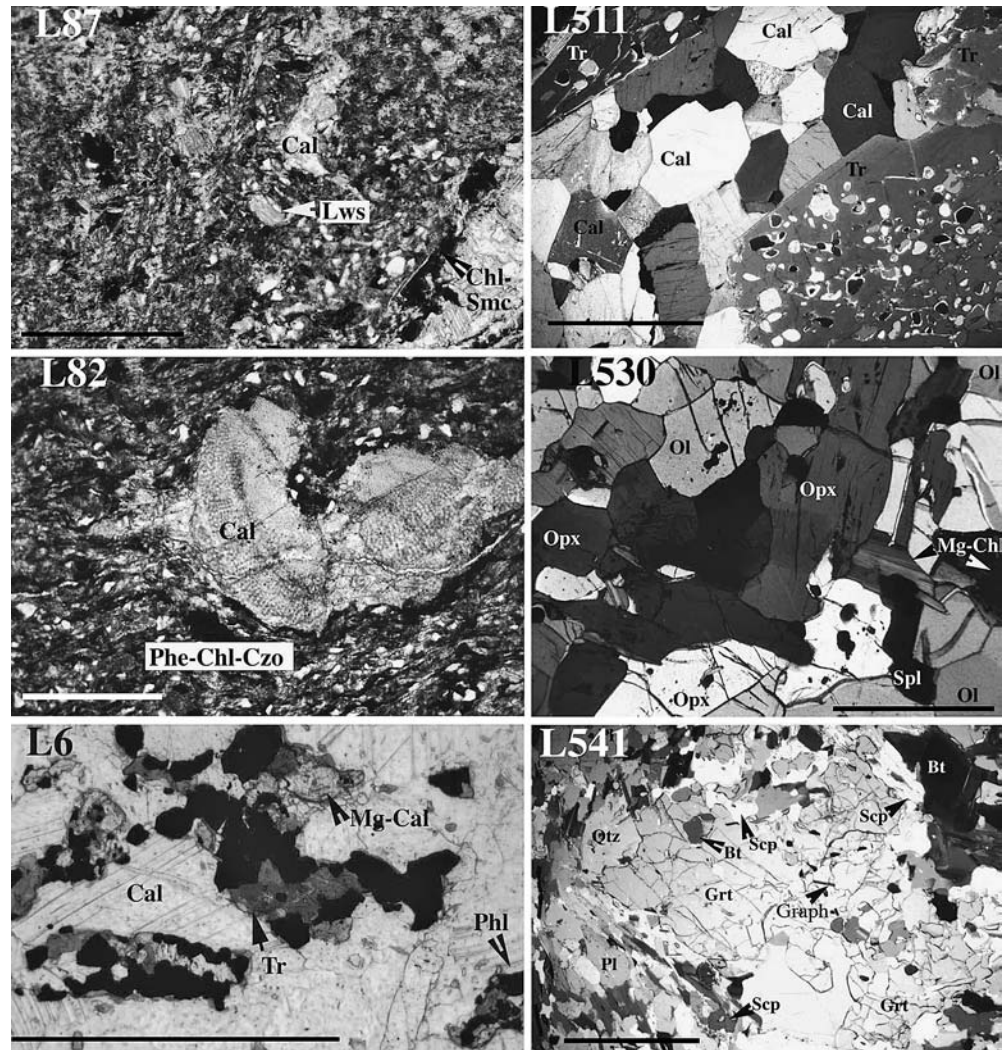
variations. Orthopyroxene is enstatite-rich (En: 91–95). Olivine is forsterite-rich (Fo: 93–97). Chlorite is Mg-rich ( $X_{Mg} = 0.95$ ). Spinel core is Fe,Cr-rich and Mg,Al-depleted [ $Cr\# (Cr/(Cr + Al + Fe^{3+})) = 0.14-0.15$ ;  $Mg\# (Mg^{2+}/(Mg^{2+} + Fe^{2+})) = 0.16-0.22$ ;  $Al_2O_3 = 0.5-2.3$  wt%]. The spinel rims are magnetite-rich with  $Cr\# \leq 0.05$ .

**Garnet-scapolite-plagioclase-biotite** In assemblage 11, garnet is weakly zoned ( $X_{alm} = 0.51-0.52$ ;  $X_{prp} = 8.9-9.1$ ;  $X_{grs} = 35.4-35.6$ ;  $X_{sps} = 4.6-3.0$ ). Scapolite is meionite rich ( $X_{me} = 0.76-0.78$ ). Plagioclase is anorthite-rich (An: 57–62). Biotite is Fe-rich ( $X_{Fe} = 0.56-0.57$ ).

### Metamorphic reactions and thermobarometry

In the lower-grade samples, X-ray analysis of sample L73 (assemblage 1) shows the presence of chlorite-smectite interlayers (Fig. 8). The presence of chlorite-smectite interlayers and the low illite crystallinity defined by the half-height width of diffraction peaks of illite (KI,

**Fig. 6** Microphotographs of the successive mineral parageneses observed with increasing metamorphic grade. Scale is 250  $\mu$ m. Mineral abbreviations are following Kretz (1983). Note that in lower-grade samples (L82 and L87) the initial sedimentary texture is preserved, with fossils, the metamorphic foliation is weak and metamorphic minerals occur as very small grains (several tens of microns). Increase in metamorphic grade results in the coarsening of calcite and other minerals (samples L6 and L511), with large poikilitic tremolite porphyroblasts. In higher-grade samples, calc-silicates restites are made of olivine + orthopyroxene (sample L530). Within migmatitic liquids, coronitic textures of scapolite + biotite around garnet porphyroclasts are observed (sample L541)

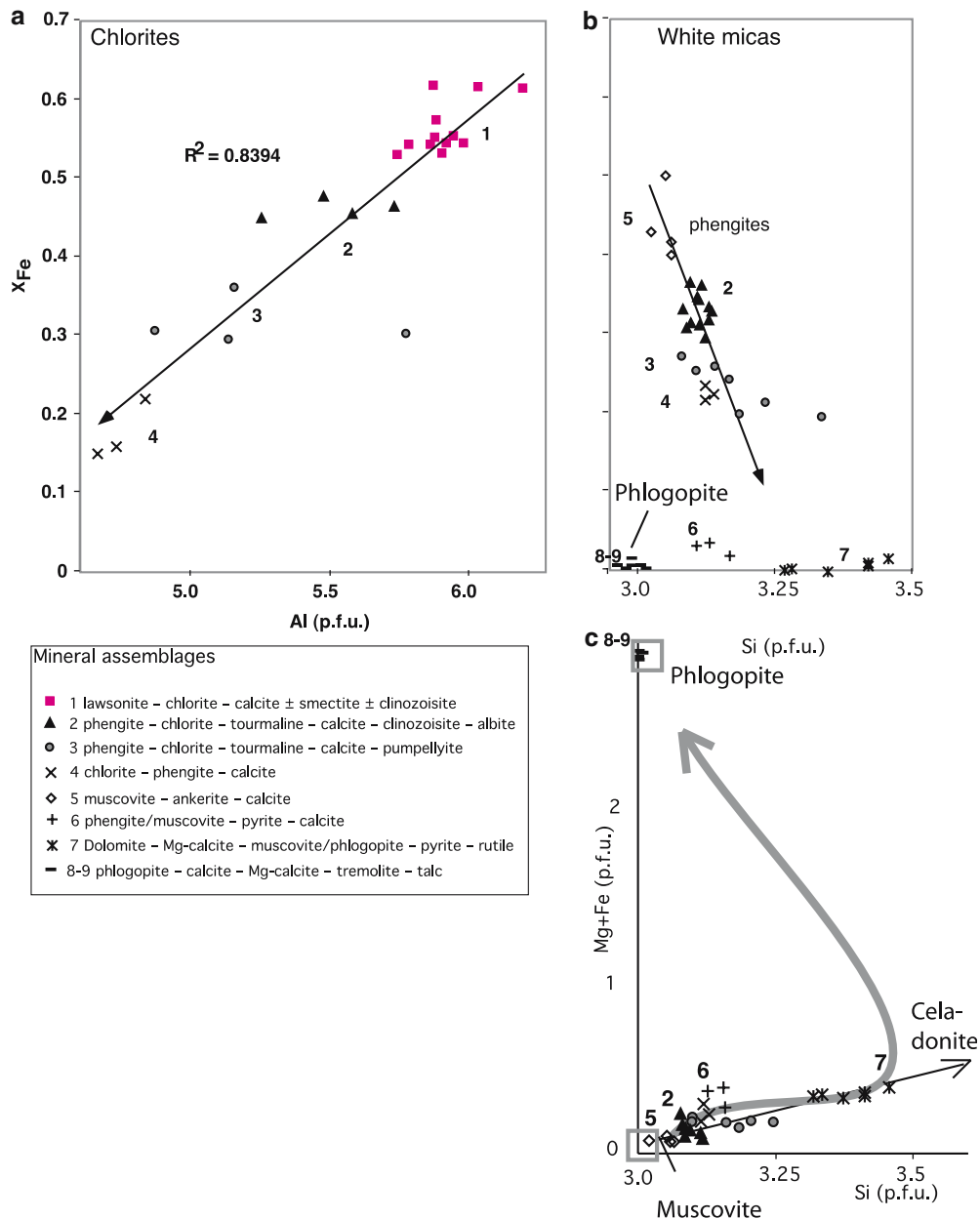


**Table 2** Representative EPMA mineral analyses of Karakoram marbles (mineral abbreviations after Kretz 1983)

Mineral	Lws	Chl	Cal	Czo	Phe	Chl	Phe	Chl	Pmp	Phe	Chl	Ms	Ank	Dol	Phl	Cal	Mg-Cal	Mg-Cal	
Assemblage	1	1	1	2	2	2	3	3	4	4	4	5	5	7	8	8	8	9	
Sample (in wt%)	L87	L87	L87	L82	L82	L82	L73	L73	L75	L75	L75	L76	L76	L160	L6	L6	L6	L6	L511
SiO <sub>2</sub>	36.27	24.67	—	39.47	46.38	25.28	49.75	26.23	33.94	47.36	29.27	44.10	—	—	41.69	—	—	—	—
TiO <sub>2</sub>	—	—	—	0.06	0.34	—	0.21	—	—	1.15	0.05	0.17	—	—	0.64	—	—	—	—
Al <sub>2</sub> O <sub>3</sub>	26.11	23.60	—	30.83	34.54	22.50	29.95	21.17	23.46	33.86	20.23	36.23	—	—	12.18	—	—	—	—
FeO	2.74	26.36	0.12	4.59	1.15	23.13	1.18	19.43	6.46	0.99	8.83	0.53	13.66	—	0.09	0.09	—	—	—
MnO	0.07	—	—	0.04	—	0.10	—	—	—	—	—	—	0.65	—	—	—	—	—	0.07
MgO	2.30	12.35	—	—	1.26	15.56	2.70	19.37	0.30	1.85	26.27	0.42	11.65	22.44	27.72	0.44	5.79	1.85	
CaO	22.52	—	60.19	22.11	—	—	0.13	0.37	18.07	—	0.09	0.22	28.91	34.01	0.33	51.74	55.05	58.80	
Na <sub>2</sub> O	—	—	—	0.11	0.32	—	—	—	—	0.26	—	0.39	—	—	0.13	—	—	—	
K <sub>2</sub> O	—	—	—	—	10.35	—	10.08	—	—	10.73	—	10.33	—	—	10.61	—	—	—	
Total	90.01	86.98	60.31	97.21	94.34	86.57	94.00	86.57	82.23	96.20	84.74	92.39	54.87	56.45	93.39	52.27	60.84	60.72	
Nb oxygen	8	28	9	13	11	28	11	28	13	11	28	11	9	9	11	9	9	9	
Si	1.87	5.31	—	3.10	3.12	5.35	3.34	5.43	3.22	3.13	5.86	3.02	—	—	2.97	—	—	—	
Al	1.59	5.98	—	2.85	2.74	5.62	2.37	5.16	2.62	2.64	4.77	2.93	—	—	1.02	—	—	—	
Fe	0.11	4.74	0.01	0.30	0.06	4.10	0.07	3.36	0.51	0.05	1.48	0.03	0.63	—	0.01	—	—	—	
Mg	0.18	3.96	—	—	0.13	4.92	0.27	5.97	0.04	0.18	7.85	0.04	0.95	1.43	2.94	0.04	0.38	0.13	
Ti	—	—	—	—	0.02	—	0.01	—	—	0.06	0.01	0.01	—	—	0.03	—	—	—	
Mn	—	—	—	—	—	0.02	—	—	—	—	—	—	0.03	—	—	—	—	—	
K	—	—	—	—	0.89	—	0.86	—	—	0.90	—	0.90	—	—	0.96	—	—	—	
Ca	1.25	—	2.99	1.86	—	—	0.01	0.08	1.84	—	0.02	0.02	1.70	1.57	0.03	2.96	2.62	2.87	
Na	—	—	—	0.02	0.04	—	—	—	—	0.03	—	0.05	—	—	0.02	—	—	—	

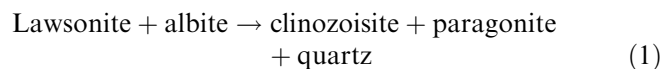


**Fig. 7** Chemical composition of Karakorum low metamorphic grade chlorites (a) and white micas (b, c). Numbers 1 to 9 refer to the successive mineral assemblages found across the metamorphic pile. The arrows indicate the direction of increasing metamorphic grade.  $X_{Fe}$  is the ratio of Fe/(Mg + Fe) recalculated as cationic contents

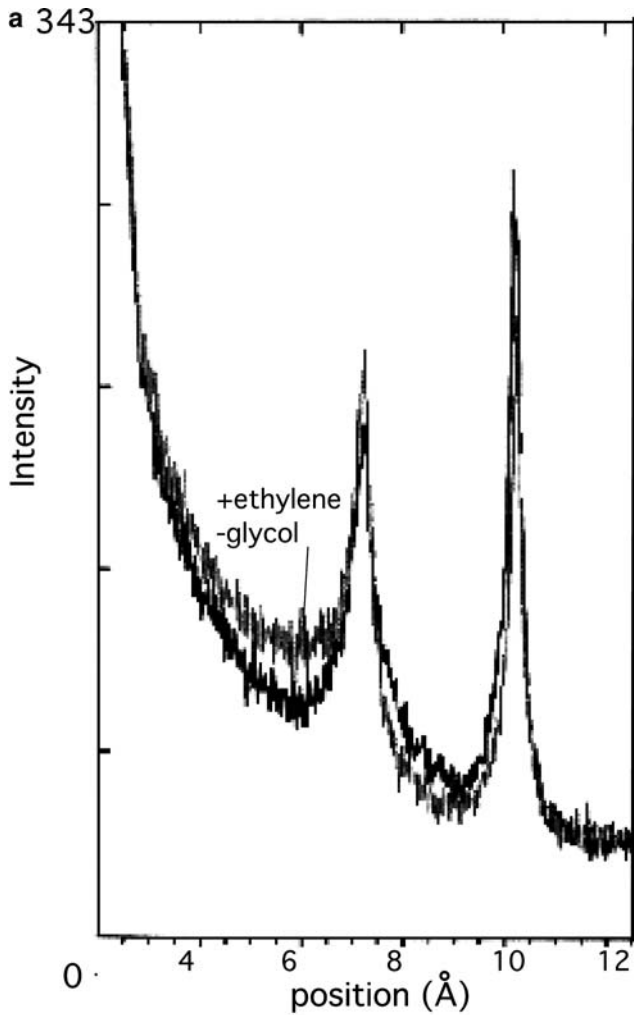


e.g. Kübler 1990; Fig. 8a) indicate low-grade metamorphic conditions. The samples span between upper anchizone to lower epizone conditions ( $0.32 > KI > 0.2$ ; Fig. 8), as defined by Kübler (1990). The stability of illite-smectite interlayers and the low phengite component (Si: 3.1–3.3 p.f.u.) suggest low-pressure conditions (below 500 MPa) according to the barometer of Masone and Schreyer (1987), which in absence of biotite and K-feldspar would yield a minimum pressure estimate. The coexistence of lawsonite and clinozoisite in assemblage 1 fixes a maximum temperature of around 350°C (Heinrich and Althaus 1988). In assemblage 2, absence of lawsonite and appearance of clinozoisite suggest its complete breakdown to clinozoisite + paragonite (interlayered within phengite), due to a slight

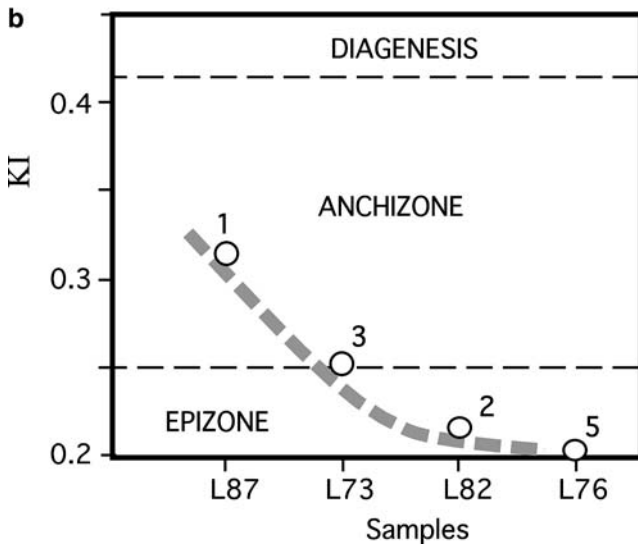
increase of temperature ( $> 350^{\circ}\text{C}$ ; Heinrich and Althaus 1988):



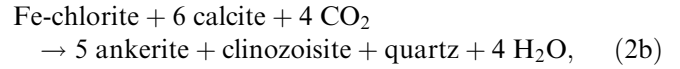
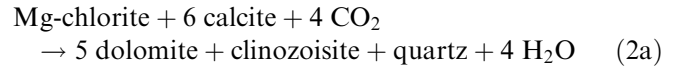
*P-T* conditions for this muscovite—chlorite ± lawsonite ± clinozoisite—bearing assemblage have been fixed using the approach detailed in Vidal and Parra (2000), based on a dataset complemented by experimental calibrations of Vidal et al. (2001). The assemblage used for the calculations is lawsonite-clinozoisite (czo: 0.8)—chlorite—phengite compositions of assemblage 2; the composition of assemblage 1 lawsonite has been used for the calculations. The result of the calculations is



**Fig. 8** X-ray diffraction characteristics of Karakorum lower-grade samples. **a** Comparison of X-ray spectra of smectite-chlorite from sample L87 (assemblage1) obtained with (grey) and without (black) ethylene-glycol added to sample L73 powder. Positions in Å are recalculated from  $2\theta$ . Indices of clay minerals are from Lanson and Meunier (1995). **b** Kübler Index (KI) of illite crystallinity in lower-grade samples. Numbers 1, 2, 3 and 5 refer to assemblages numbers, and samples are also indicated (L73-87)

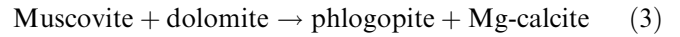


Fe/Mg-rich calcite could be accounted for by the following reactions:

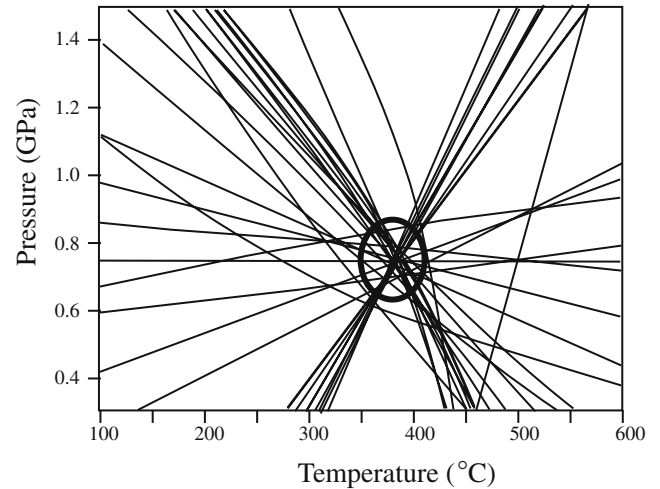


depending on the initial Fe and Mg contents of the rock.

The breakdown of muscovite, and appearance of phlogopite, together with a transition from dolomite to Mg-calcite, suggest the following reaction:



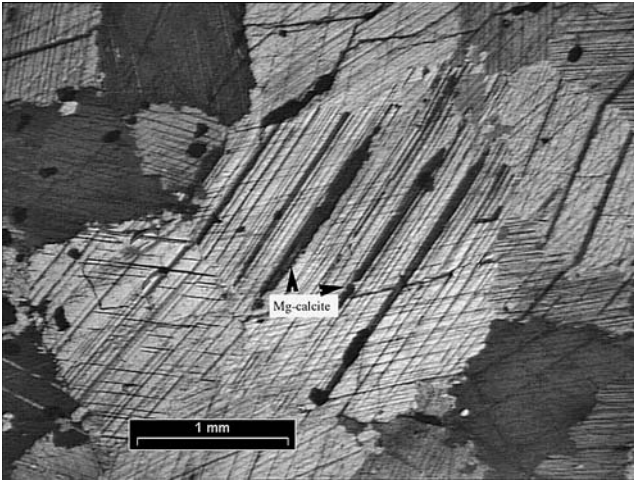
As shown by Goldsmith and Heard (1961) and Goldsmith and Newton (1969), the dolomite-calcite solvus is well-known as a geothermometer for LP dolomitic marbles because of the small pressure dependence of  $\text{MgCO}_3$  solubility in calcite. To calculate the temperature, we have used the following equation after Sheppard and Schwarcz (1970):



**Fig. 9** Pressure-temperature diagram showing mineral equilibria for the M1 assemblage of sample L82 (assemblage 2), computed in the CKFMASH system. The diagram was computed with the TWEAQ program, assuming  $X_{\text{H}_2\text{O}} = 1$ , with the assemblage lawsonite-clinozoisite (czo: 0.8)-chlorite-phengite with mineral compositions of sample L82, using the methods and thermodynamic dataset of Vidal and Parra (2000) and Vidal et al. (2001). For methods and procedures, the reader is referred to Vidal and Parra (2000) and references therein

depicted in Fig. 9.  $P$ - $T$  conditions can be estimated at  $380 \pm 30^\circ\text{C}$  and  $0.73 \pm 0.1 \text{ GPa}$  ( $2\sigma$ ).

The breakdown of chlorite (from assemblage 5 to higher-grade ones), and the occurrence of dolomite or



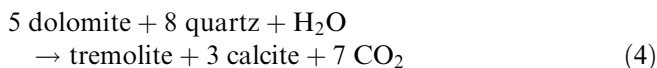
**Fig. 10** Microphotograph of calcite grains in sample L6, showing Mg-rich lamellae exsolved in the calcite

$$\begin{aligned} \text{Log MgCO}_3(\text{mol\% in calcite}) \\ = 1.727 \times 10^{-3} \times T - 0.233 \end{aligned}$$

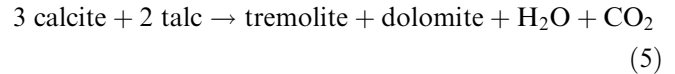
$$(400\text{C} < T < 1075\text{C})$$

Mg-calcite was found in the transition zone samples (L6 and L511, assemblages 8 and 9). However, in sample L6, Mg-calcite grains are found to have heterogeneous compositions, which could be explained by incomplete diffusion of Mg in a rapidly growing calcite at the expense of small dolomite inclusions (Ogasawara et al. 1998). The observed compositional pattern is that of lamellae with Mg-rich calcite (Mg = 1.8–5.8 wt%) within a Mg-poor calcite crystal (Mg = 0.4–0.6 wt%) (Fig. 10). Following the approach of Puhan (1976), we estimated the composition of the primary calcite grain using the surface area of each of the Mg-rich and Mg-poor calcite components. Surface areas have been estimated using the software developed at the U.S. National Institutes of Health (NIH, image 1.61, available at <http://rsbweb.nih.gov/mih-image/>). From these estimations, the Mg-poor calcite phase occupies 89% of the surface of calcite. We calculated the initial composition of the Mg-calcite of  $X_{\text{MgCO}_3} = 3.49 \text{ mol\%}$  from the surface ratio of each component and its EMPA composition (Table 2). This value yields a minimum temperature estimate of 450°C. In sample L511, very sharp mineral contacts are observed, with a relatively homogeneous calcite composition ( $X_{\text{MgCO}_3} = 0.04 - 0.06$ ). Using the highest MgCO<sub>3</sub> content in calcite, the (minimal) estimated temperature is 570°C.

Reaction 3 was closely followed or even accompanied by a tremolite-in / dolomite-out reaction:



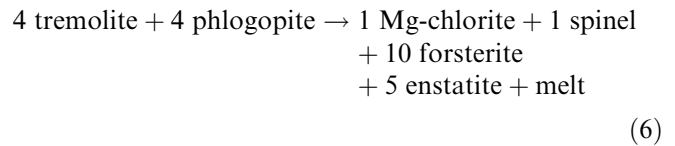
Within the tremolite porphyroblasts of assemblage 9, talc is present as rounded relict grains, suggesting the reaction:



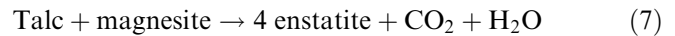
Other reactions involving talc and producing tremolite can be proposed (see Letargo et al. 1995).

Within the high-grade M2 area, the orthopyroxene-olivine-spinel-Mg chlorite assemblage in ultramafic pods (samples L530 and L563) developed at the expense of lower-grade minerals (e.g. talc, Fig. 6), thus featuring a prograde PT evolution. We have estimated a temperature of 815–850°C using the olivine-orthopyroxene-spinel thermometer of Wells (1977), in agreement with experimental data of Boyd (1959).

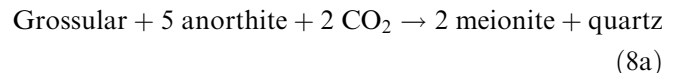
The transition from assemblage 9 to assemblage 10, suggests the loss of a Ca-rich component presumably through melt segregation:



The melt component calculated by mass-balance calculation is: 25 SiO<sub>2</sub> + 4.5 O<sub>2</sub> + 4 CaO, which is in agreement with field observations of quartz-calcite matrix surrounding ultramafic pods. The presence of magnesite and talc relicts within late orthopyroxene porphyroblasts (Fig. 6) suggests the following prograde reaction:

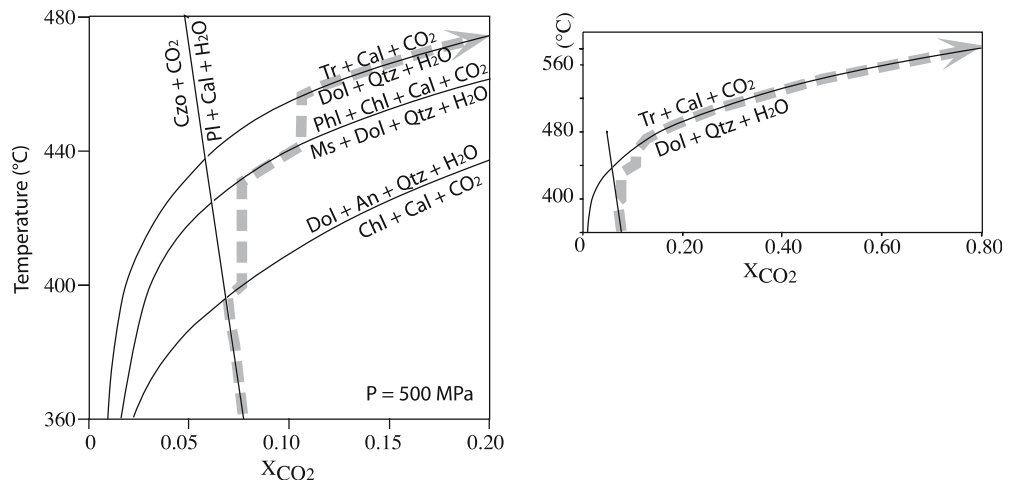


In the migmatite layers of the dome core (sample L541, assemblage 11), the development of meionitic scapolite as coronas around grossular garnet and the crystallisation of graphite (Fig. 6) are consistent with a prograde HT reactions involving consumption and reduction of a CO<sub>2</sub>-rich fluid:



Peak-temperature assemblages can be used only to fix broadly the peak metamorphic conditions (Harley et al. 1994). However, grossular breakdown reaction 8a has been calculated and experimentally constrained at temperatures between 790 and 830°C at 0.5 GPa (Goldsmith 1976; Satish-Kumar et al. 1996). Similar temperatures are expected for the meionite assemblage of the domes area, as pressure estimates from the interlayered metapelites are similar to experimental ones (0.55 GPa; Rolland et al. 2001); however, the meionite stability field depends also on the value of  $X_{\text{CO}_2}$  (Goldsmith 1976).

**Fig. 11** Isobaric  $T$  versus  $X_{\text{CO}_2}$  diagram, modified after Bucher and Frey (1994), showing the evolution of  $X_{\text{CO}_2}$  pore fluid composition with increasing temperature during M1 as deduced for the marls from lower metamorphic zones



### Constraints on the nature of fluids ( $X_{\text{CO}_2}, f_{\text{O}_2}$ )

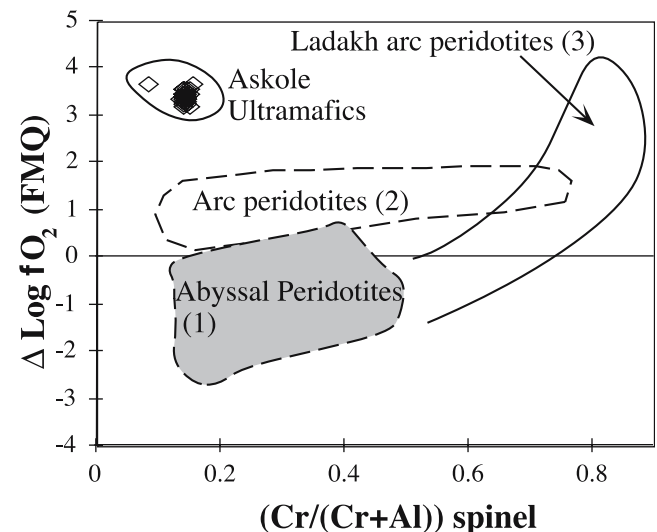
For the low grade samples,  $X_{\text{CO}_2}$  can be fixed using the grids in the KCMAS-HC system (Fig. 11) defined by Bucher and Frey (1994). At 350–400°C (temperature imposed by the lawsonite-clinozoisite transition), the clinozoisite-out, chlorite-out, muscovite-out and tremolite-in reactions impose low  $X_{\text{CO}_2}$  values in the isobaric grids of the KCMAS-HC system (Fig. 11) defined by Bucher and Frey (1994), i.e. values of about 0.01 at 360°C increasing progressively to 0.11 at 450°C (peak temperature of the assemblage 8). The preservation of tremolite + talc from assemblage 8 to 9 suggests that the same  $\text{CO}_2$ -producing reaction was followed in the  $T - X_{\text{CO}_2}$  space, and that  $X_{\text{CO}_2}$  increased dramatically with metamorphic grade between these two locations. The highest temperature estimated for the assemblage 9 (570°C) imposes very high  $X_{\text{CO}_2}$  of 0.8 following the extrapolation of tremolite-in reaction curve of Fig. 11. This metamorphic evolution is consistent with a model of closed system behaviour down to that part of the metamorphic pile.

In the high-grade zone, the partial melting and migmatization of calcic and pelitic lithologies producing restites and mobilisates (e.g. Fig. 2d) suggest a transition to a more open-system behaviour. The assemblage olivine-pyroxene-spinel in ultramafic boudins can also be used to derive the value of  $\Delta \text{Log} f_{\text{O}_2}$  in these lithologies. Following the  $\Delta \text{Log} f_{\text{O}_2}$  barometer of Ballhaus et al. (1991), based on the composition of the coexisting minerals of this assemblage, the oxygen fugacity values obtained range between 3.0 and 3.6 units relative to the FMQ (fayalite-magnetite-quartz) buffer. These values are in agreement with the very low Cr# [Cr/(Cr + Al)] ratios of spinel (0.1–0.2), which differ from the values for spinel from oceanic arc and abyssal peridotites (Parkinson and Arculus 1999; Rolland et al. 2002a; Fig. 12). The Cr# and  $\Delta \text{Log} f_{\text{O}_2}$  values of Askole ultramafics are much higher compared to oceanic ultramafics, which is a proof of their metamorphic origin in a continental setting during the Himalayan M2 stage (Fig. 12). This

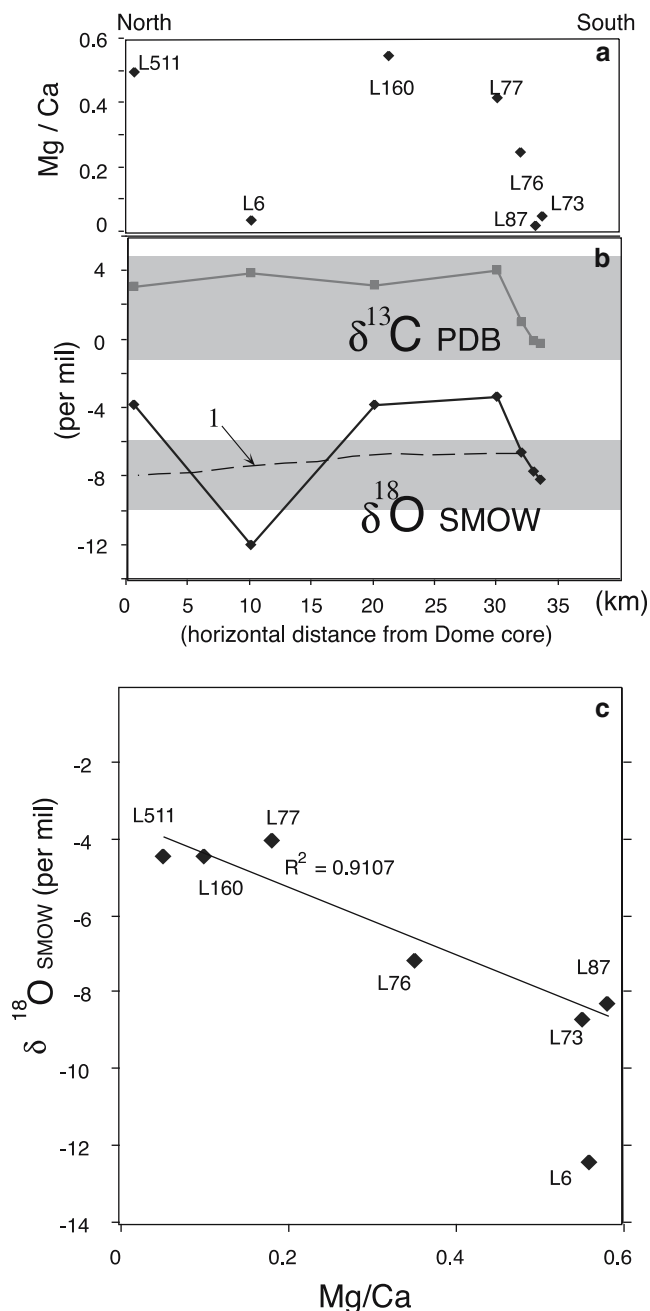
value is consistent with  $\text{O}_2$  release during reaction 6 and other muscovite and biotite decompression melting reactions in the interlayered metapelites (Rolland et al. 2001). Subsequently,  $X_{\text{CO}_2}$  values decreased during the transition from assemblage 9 to 10. Concerning the migmatites, the presence of meionitic scapolite implies minimum  $X_{\text{CO}_2}$  values of 0.50 (Satish-Kumar et al. 1996) at the pressure value of 0.55 GPa estimated from the metapelites (Rolland et al. 2001). It is likely that these high  $X_{\text{CO}_2}$  values in the melt are due to mixing with marbles during melting, which is shown by field relationships (Fig. 2d).

### Geochemistry

The analysed Karakorum carbonates range between Si-Al rich pelitic limestone (e.g. L67:  $\text{SiO}_2 = 36.1 \text{ wt}\%$ ;



**Fig. 12** Spinel Cr# and oxygen fugacity ( $\Delta \text{Log} f_{\text{O}_2}$ ) values of Askole ultramafic bands. For the data of the fields 1 (abyssal peridotites) and 2 (arc peridotites) see Parkinson and Arculus (1999), and 3 (Ladakh arc peridotites), see Rolland et al. (2002a)



$\text{Al}_2\text{O}_3 = 10.8 \text{ wt}\%$ ;  $\text{CaO} = 27.5 \text{ wt}\%$ ) and nearly pure marble (e.g. L77:  $\text{SiO}_2 = 0.02 \text{ wt}\%$ ;  $\text{Al}_2\text{O}_3 = 0.17 \text{ wt}\%$ ;  $\text{CaO} = 55.3 \text{ wt}\%$ ; Table 3). Major element analyses of the metamorphic series show a progressive increase of Mg and a relative decrease of Ca contents from the low-grade to the transition zone (Fig. 13a), except sample L6. Other variations in major elements, such as the Fe, Mn contents, are not clearly related to the metamorphic grade, and are thought to reflect variation of the initial sedimentary compositions.

Carbon isotope compositions of carbonates ( $\delta^{13}\text{C}_{\text{PDB}}$ , Table 3, Fig. 13b) are in good agreement with sedimentary limestone values obtained for the Cambro-Ordovician period (e.g. Rolland et al. 2002b). In

contrast, carbonate oxygen isotope ratios ( $\delta^{18}\text{O}_{\text{SMOW}}$ ) increase with metamorphic grade (except for sample L6), and exceed the range predicted for sedimentary (including diagenetically modified) values derived from carbonate sediments with corresponding  $\delta^{13}\text{C}$  values (Fig. 13b). There is a good linear correlation of  $\delta^{18}\text{O}$  with Mg/Ca ratios ( $R^2 = 0.91$  except sample L6; Fig. 13c), which indicates that the increases in  $\delta^{18}\text{O}$  and Mg/Ca ratios are due to a process of increasing temperature during a diagenetic or metamorphic event. More data should be obtained to discriminate between these two processes.

## Discussion

The study of carbonates from the KMC provides both further understanding of the metamorphic evolution of the Karakorum margin, and insights into the roles

**Table 3** Major element analyses and stable isotopic composition of Karakorum marbles

	L76	L77	L73	L87	L6	L160	L511
$\text{SiO}_2$	34.84	0.01	13.2	36.09	36.22	36.99	10.82
$\text{TiO}_2$	1.3	0.01	1.71	0.61	1.2	0.66	0.08
$\text{Al}_2\text{O}_3$	13.9	0.167	3.42	10.8	9.78	10.92	4.18
$\text{Fe}_2\text{O}_3$	10.46	–	1.16	4.59	3.67	7.44	0.99
MnO	1.6	–	0.26	0.26	0.02	1.27	0.02
MgO	2.6	0.45	1.17	1.25	0.92	4.8	11.33
CaO	15.44	55.34	58.01	27.51	25.06	8.17	31.82
$\text{Na}_2\text{O}$	–	0.17	–	0.49	1.04	1.34	0.48
$\text{K}_2\text{O}$	4.54	0.13	0.84	1.14	1.01	1.02	0.44
$\text{P}_2\text{O}_5$	0.49	0.02	1.16	0.69	0.07	1.5	0.01
LOI	14.36	43.26	19.85	17.2	21.2	27.18	39.58
Total	99.53	99.56	100.78	100.63	100.19	101.29	99.75
$\delta^{18}\text{O}_{\text{SMOW}}$	–7.17	–3.99	–8.27	–8.67	–12.42	–4.43	–4.44
$\delta^{13}\text{C}_{\text{PDB}}$	1.09	4.03	–0.04	–0.22	3.06	3.13	3.85

played by diffusion and advection of heat during an orogenic event. Concerning the relative extent of the two major metamorphic events (M1 and M2), the data presented here complement the pre-existing thermobarometric estimates provided by studies on the metapelitic lithologies of the kyanite-staurolite and sillimanite bearing metapelites of the KMC (Bertrand et al. 1988; Searle et al. 1989; Allen and Chamberlain 1991; Lemennicier et al. 1996; Rolland et al. 2001).

### M1 Event

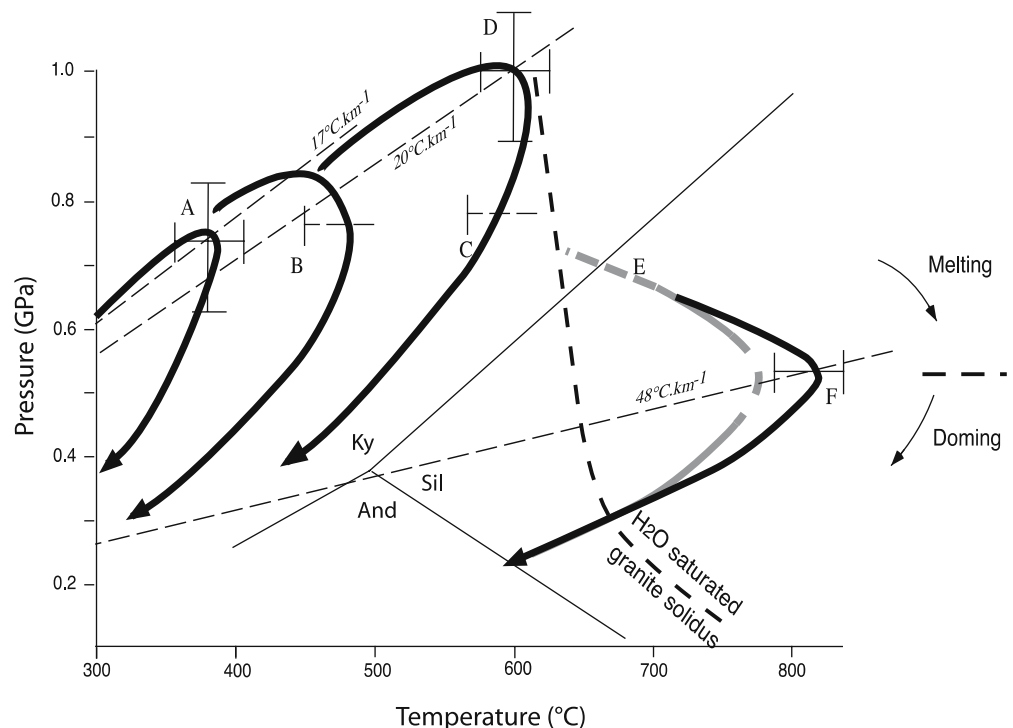
Concerning the M1 event, our  $P$ - $T$  estimates document for the first time a metamorphic field gradient from (a) upper anchizone conditions ( $T < 350^\circ\text{C}$ ;  $P < 0.5$  GPa) to (b) LT-MP conditions ( $T = 380^\circ\text{C}$ ;  $P = 0.73$  GPa) and to (c) MT-MP conditions ( $T = 600^\circ\text{C}$ ;  $P = 1.0$  GPa) towards the north (Fig. 14). LT-MP conditions reflect a low thermal gradient ( $17^\circ\text{C km}^{-1}$ ). This low thermal gradient, evidenced by the first metamorphic record of lawsonite/clinozoisite-bearing lithologies along the south Karakorum margin is in agreement with subduction-related geotherms elsewhere in the Alpine orogen (e.g. Spalla et al. 1996). These LT-MP conditions are clearly compatible with the subduction of the Kohistan-Ladakh back-arc domain under the Karakorum margin, which is the only subduction event known along the South Karakorum margin (Rolland et al. 2000). These data are also in good agreement with the partial resetting of Ar-Ar amphibole ages during the early Himalayan history (65–20 Ma) in the Proterozoic, Triassic and Cretaceous rocks of the lower-grade Karakorum

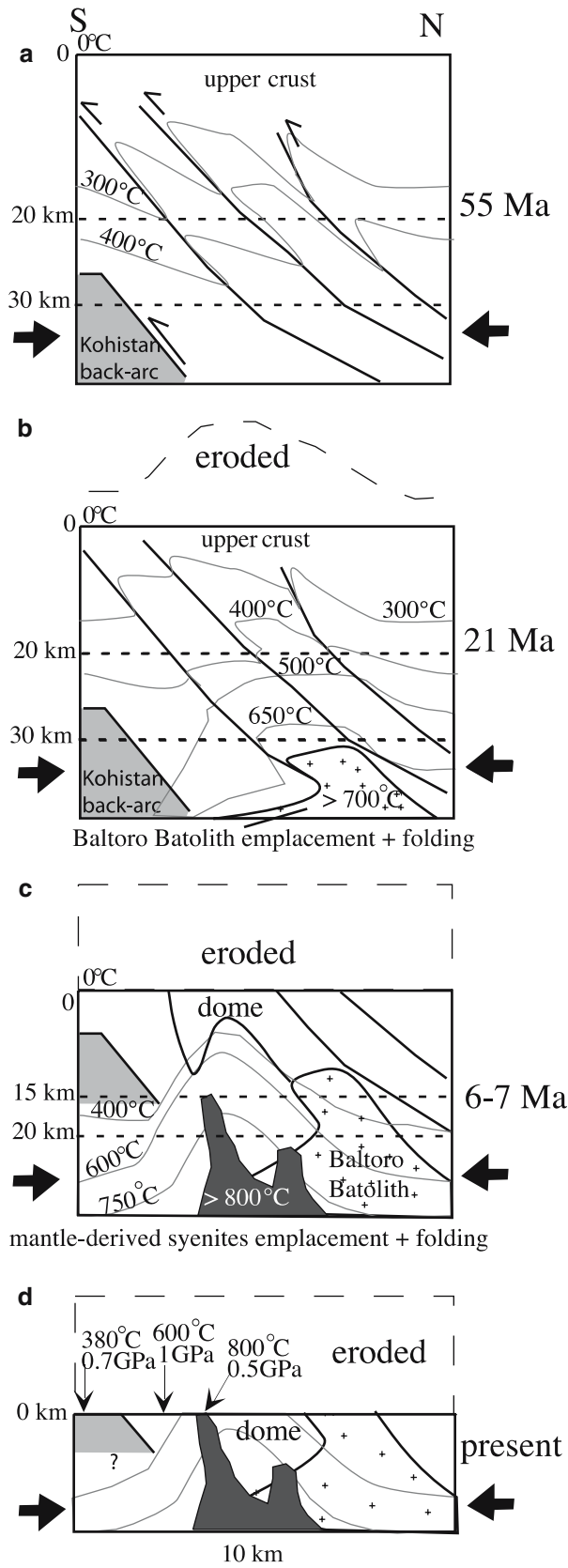
area (Rolland et al. 2002b, 2005). Progressive increase in  $P$ , and more significantly in  $T$  conditions to the north of the structural section, suggest a transition towards more Barrovian syn-stacking metamorphism.

### M2 Event

Thermometry conducted on M2 assemblages of meionite scapolite-bearing calc-silicates and ultramafic rocks yields temperatures between  $790$  and  $850^\circ\text{C}$ . These estimates are slightly higher than those obtained on metapelitic migmatites ( $T = 776 \pm 10^\circ\text{C}$ ; Rolland et al. 2001). In other high-grade terrains where granulite-grade marbles have been studied in detail (e.g. South India), meionitic scapolite is generally retrogressed to grossular or plagioclase + calcite symplectites (e.g. Satish-Kumar et al. 1996). Here, the rimming of grossular by meionitic scapolite (reaction 8a) is the result of a prograde reaction (e.g. Goldsmith 1976; Satish-Kumar et al. 1996). In the pelitic lithologies, the preservation of prograde HT metamorphic features is locally observed at the margin of the high-grade zone, before the onset of migmatitisation (staurolite is still present while sillimanite occurs in contact with kyanite; Rolland et al. 2001). In contrast, metapelites within the domes have been partly reequilibrated through back-reaction with the melt during cooling (e.g. White and Powell 2002). Consequently, the temperature of  $790$ – $850^\circ\text{C}$  estimated from the ultramafic and calc-silicate parageneses should therefore be the closest estimate of the temperature peak (Fig. 14f, g). This high M2 temperature peak occurred at relatively low-pressure conditions ( $0.5$ – $0.6$  GPa) and

**Fig. 14**  $P$ - $T$  paths in various locations of the Karakorum margin. **a**  $P$ - $T$  conditions of assemblage 1; **b**  $P$ - $T$  estimate from assemblage 2; **c**, **d**  $T$  estimates derived from assemblages 7 and 8, respectively, with  $P$  conditions ranging between **b** and **e**; **e** maximum  $P$ - $T$  conditions obtained for the M1 metamorphic event (Lemennicier et al. 1996; Rolland et al. 2001); **f**  $P$ - $T$  path of the core of M2 domes as constrained from the study of metapelites (Rolland et al. 2001); **g** temperature conditions estimated from calc-silicate and ultramafic lithologies in the core of the Askole M2 dome





only at 6–7 Ma (U–Pb zircon age in metapelites of the Dasso Dome by Smith 1993). Complete metamorphic

**Fig. 15** Geodynamic reconstitution of the tectonic and thermal evolution of the Karakorum crust during the Himalayan orogeny. **a** Southward thrusting of Karakorum units over the Kohistan back-arc, metamorphism M1 at pressure peak. **b** Erosion and thermal relaxation of previously thickened crust, emplacement of the Baltoro granite batholith, metamorphism M1 at temperature peak (700°C). **c** Erosion and metamorphic dome emplacement by folding of the previously relaxed thickened crust, emplacement of mantle-derived high-K syenites of Hemasil, and M2 temperature peak (> 800°C). **d** erosion and current exposure of the various rock types, with the paleo-temperatures and pressures obtained by thermobarometry

reequilibration during M2 is very restricted in space in the KMC (several km<sup>2</sup> in Dasso and Askole dome cores). This restricted metamorphic reequilibration is also reflected by Ar–Ar mineral dating, which shows increased resetting of pre-Himalayan ages towards the M2 high-grade zone, in the so-called Transition zone, with partial to complete resetting of Ar–amphibole ages between 20 and 11 Ma (Rolland et al. 2005).

#### Geodynamic interpretation

In the 17-km-wide southern Karakorum margin, from the lower-grade zone to the transition zone, the horizontal difference in peak temperature is  $\delta T \geq 300^\circ\text{C}$  (from South to North). The geothermal gradient in the southern lower-grade part would be  $17^\circ\text{C km}^{-1}$ , and  $20^\circ\text{C km}^{-1}$  in the upper-grade northern part (during the M1 event). These values, and the shape of the M1 *P-T* paths, with a metamorphic peak well below the temperature of the granulite facies, are in agreement with models of subduction-related metamorphism with large rates of convergence (Jamieson et al. 2002). This phase of tectonic stacking has occurred during the first stage of the Karakorum mountain building, since the Upper Cretaceous with the subduction of the Kohistan-Ladakh back-arc, and more intensely since 55 Ma with the onset of the India–Asia collision (Fig. 15a). As suggested by preserved syn-stacking LT-MP mineral assemblages (300–380°C) at the lower part of the metamorphic pile, it seems that thermal reequilibration of the Karakorum crust is very slow after the collisional event. The preservation of Eo-Himalayan metamorphic assemblages in the lower part of the structural pile advocate for low fluid/rock ratios, and slow fluid circulation in a diffusion-dominated environment. The initial sedimentary <sup>13</sup>C/<sup>12</sup>C signature of marbles has been preserved in the lower part of the pile, showing that metamorphism has not affected that part of the KMC. As emphasised in the geochemistry section, the trend observed in the  $\delta^{18}\text{O}$  versus Mg/Ca diagram (Fig. 15c) reflects an increase of temperature during either a sedimentary-diagenetic or the M1 metamorphic event. This slow partial reequilibration has led to amphibolite-grade metamorphism in the upper part of the pile (600°C–1.0 GPa) and to the partial melting of metapelites and calc-silicates that were

previously underthrust at lower crust levels, and emplacement of the Baltoro granite batholith at c. 21 Ma (Fig. 15b).

This diffusion-dominated metamorphic style ceased at 6–7 Ma, with the emplacement of mantle-derived syenites and coeval HT metamorphism (Fig. 15c). The preservation of pre-M2 metamorphic conditions and  $\delta^{18}\text{O}$  values close to the domes (Transition zone), the sharp contacts between migmatites and amphibolites, show that the boundary between diffusional and advective thermal domains was very sharp (Fig. 15c, d). From the margin to the core of the high-grade zone, the increase in recorded maximal temperature conditions is  $\delta T \geq 200^\circ\text{C}$ . Peak temperature conditions are in agreement with a geothermal gradient of  $48^\circ\text{C km}^{-1}$  prevailing in the core of the domes zone during the M2 event, which is a common feature in thermally relaxed fossil orogens such as the Variscan Chain (e.g. Gardien et al. 1997). This sharp transition is currently imaged geophysically by an E–W zone of negative Bouguer anomaly above the high-grade zone (Caporali 2000), and by a zone of higher mountain elevations from the Nanga Parbat–Haramosh massif to the area of the 8,000 m peaks (K2, Broad Peak, Gasherbrum). The limited spatial extension of M2 metamorphic re-equilibration could be ascribed to rapid exhumation. The average uplift rate deduced from the drop in pressure conditions from late M1 (21 Ma) to M2 (6 Ma) metamorphic peaks ( $\Delta P = 0.5 \text{ GPa}$ ) is in the order of  $1 \text{ mm year}^{-1}$ . Subsequently, the average uplift rate of the last 6 Ma is bracketed within  $2.5\text{--}3 \text{ mm year}^{-1}$ . Such an acceleration of uplift rates and doming, can be related to the gravitational instability of homogeneously thickened crust due to the lowering of crustal density following high-temperature granulite facies metamorphism (Gerya et al. 2001). In the case of the Karakorum, this instability is clearly related to mantle-derived magmatism, which suggest a process of crustal heating possibly related to Indian slab break off since c. 20 Ma (Rolland et al. 2001; Mahéo et al. 2002).

### Concluding remarks

The source of heat for the M2 metamorphism is clearly derived from the mantle, as shown by the mantellic (Hf, Nd) isotopic signatures of synchronous syenitic magmatism, which is spatially associated with the HT rocks, possibly in response to Indian slab break off at c. 20 Ma (Rolland et al. 2001; Mahéo et al. 2002). This upward flow of mantle-derived magmas in a currently shortening context shows that advective heat flow from the mantle is possible even at shallow levels (0.5 GPa—15 km) in the crust of thickened orogens. This observation questions the hypothesis that the onset of HT metamorphism is due to extensional tectonics after the thermal relaxation of thickened continental crust in fossil orogens such as the Hercynian orogen (eg. Gardien et al. 1997 and

references therein). In the light of the tectono-metamorphic evolution of the KMC, we can suggest that the processes of thermal transfer in an active and currently still thickening, orogen are also very heterogeneous. Advective heating might be the result of crustal-scale features such as folds and faults, which act as drains for the flow of fluids, magmas and thus heat. As shown in the Karakorum crust, the boundary between these advective and diffusion-dominated domains is very sharp at mid-crustal levels, and LP-granulite grade metamorphism can predate the stages of post-collisional extension. The example of the Karakorum shows that advective heating derived from tectonic processes such as slab break off may accelerate the process of a merely diffusional thermal relaxation of the crust by focused intrusion of mantle-derived magmas.

**Acknowledgements** We greatly acknowledge the help of the Geoscience Laboratory during fieldwork and preliminary lab work. Fieldwork was supported by the LGCA (Grenoble), during the Ph.D. of the first author. We greatly acknowledge the help of F. Keller during the acquisition of major element data, M. Veschambre for her assistance during electron microprobe analysis, and fruitful discussions with O. Vidal, S. Guillot, G. Mahéo and P. Treloar. The paper benefited from the reviews of Dr Taras Gerya and Pr Somnath Dasgupta, and from editorial handling by Pr Raith.

### References

- Allen T, Chamberlain CP (1991) Metamorphic evidence for an inverted crustal section, with constraints on the Main Karakorum Thrust, Baltistan, northern Pakistan. *J Metamorph Geol* 9:403–418
- Anovitz LM, Essene EJ (1987) Phase equilibria  $\text{CaCO}_3\text{-MgCO}_3\text{-FeCO}_3$ . *J Petrol* 28:389–414
- Aucour AM, Sheppard SMF, Guyomar O, Wattelet J (1999) Use of  $^{13}\text{C}$  to trace origin and cycling of inorganic carbon in the Rhône river system. *Chem Geol* 159:87–105
- Ballhaus C, Berry RF, Green DH (1991) High pressure experimental calibration of the olivine-orthopyroxene-spinel oxygen barometer: implications for the oxidation state of the mantle. *Contrib Mineral Petrol* 107:27–40
- Bertrand JM, Kienast JR, Pinardon JL (1988) Structure and metamorphism of the Karakorum gneisses in the Braldu-Baltoro Valley (North Pakistan). *Geodin Acta* 2:135–150
- Bowen NL (1940) Progressive metamorphism of siliceous limestones and dolomite. *J Geol* 48:225–274
- Boyd FR (1959) Hydrothermal investigations of the amphiboles. In: Abelson PH (ed) *Research in geochemistry*. Wiley, New York, pp 110–215
- Bucher K, Frey M (1994) *Petrogenesis of metamorphic rocks*. Springer, Berlin Heidelberg New York, p 318
- Burkhard M (1993) Calcite twins, their geometry, appearance and significance as stress-strain markers and indicators of tectonic regime: a review. *J Struct Geol* 15:351–368
- Caporali A (2000) The gravity field of the Karakorum Mountain Range and surrounding areas. In: Khan MA, Treloar PJ, Searle MP, Jan MQ (eds) *Tectonics of the Nanga Parbat Syntaxes and the Western Himalaya* (eds) Geological Society of London Special Publications 170:7–23
- Deer WA, Howie RA, Zussman J (1996) *The rock-forming minerals*, 2nd edn. Longman, London, p 696
- Evans MA, Dunne WM (1991) Strain factorization and partitioning in the North Mountain thrust sheet, central Appalachians, USA. *J Struct Geol* 13:21–36



- Ferrill DA (1991) Calcite twin widths and intensities as metamorphic indicators in natural low-temperature deformation of limestone. *J Struct Geol* 13:667–676
- Ferry JM, Gerdes ML (1998) Chemically reactive fluid flow during metamorphism. *Ann Rev Earth Planet Sci* 26:255–287
- Gardien V, Lardeaux JM, Ledru P, Allemand P, Guillot S (1997) Metamorphism during late orogenic extension: insights from the French Variscan Belt. *Bull Soc Géol France* 168:271–286
- Gerya TV, Maresch WV, Willner AP, Van Reenen DD, Smit A (2001) Inherent gravitational instability of thickened continental crust with regionally developed low- to medium-pressure granulite facies metamorphism. *Earth Planet Sci Lett* 190:221–235
- Goldsmith JR (1976) Scapolites, granulites, and volatiles in the lower crust. *Geol Soc Am Bull* 87:161–168
- Goldsmith JR, Heard HC (1961) Subsolidus phase relations in the system  $\text{CaCO}_3\text{-MgCO}_3$ . *J Geol* 69:45–74
- Goldsmith JR, Newton RC (1969) P-T-X relations in the system  $\text{CaCO}_3\text{-MgCO}_3$  at high temperatures and pressures. *Am J Sci* 267A:160–190
- Groshong RHJ, Pfiffner OA, Pringle LR (1984) Strain partitioning in the Helvetic thrust belt of eastern Switzerland from the leading edge to the internal zone. *J Struct Geol* 6:15–18
- Hanson CR (1989) The northern suture in the Shigar valley, Baltistan, northern Pakistan. *Geol Soc Am Spec Paper* 232:203–215
- Harley SL, Fitzsimons ICW, Buick IS (1994) Reactions and textures in wollastonite-scapolite granulites and their significance for pressure-temperature-fluid histories of high-grade terranes. *Precambrian Res* 66:309–323
- Heinrich H, Althaus E (1988) Experimental determination of the reactions  $4 \text{ lawsonite} + 1 \text{ albite} = 1 \text{ paragonite} + 2 \text{ zoisite} + 2 \text{ quartz} + 6 \text{ H}_2\text{O}$  and  $4 \text{ lawsonite} + 1 \text{ jadeite} = 1 \text{ paragonite} + 2 \text{ zoisite} + 2 \text{ quartz} + 6 \text{ H}_2\text{O}$ . *Neues Jahrbuch Mineralogisch Monashefte* H11:516–528
- Jamieson RA, Beaumont C, Nguyen MH, Lee B (2002) Interaction of metamorphism, deformation and exhumation in large convergent orogens. *J Metamorph Geol* 20:9–24
- Kretz R (1983) Symbols for rock-forming minerals. *Am Mineral* 68:277–279
- Kübler B, Jaboyedoff M (2000) Illite crystallinity. *Comptes Rendus Académie des Sciences Paris* 331:75–89
- Lanson B, Meunier A (1995) La transformation des interstratifiés ordonnés illite-smectite en illite dans les séries diagénétiques. Etat des connaissances et perspectives. *Bulletin des Centres de Recherche Exploitation-Production, Elf-Aquitaine* 19:1–15
- Le Fort P (1975) Himalaya: the collided range, present knowledge of the continental arc. *Am J Sci* 275A:1–44
- Le Fort P, Tongiorgi M, Gaetani M (1994) Discovery of a crystalline basement and Early Ordovician marine transgression in the Karakorum mountain range, Pakistan. *Geology* 22:941–944
- Leake BE, Wooley AR, Arps CES, Birch WD, Gilbert MC, Grice JD, Hawthorne FC, Kato A, Kisch HJ, Krivovichev VG, Linthout K, Laird J, Mandarino JA, Maresch WV, Nickel EH, Rock NMS, Schumacher JC, Smith DC, Stephenson NCN, Ungaretti L, Whittaker EJW, Guo Youzhi (1997) Nomenclature of amphiboles: report of the Subcommittee on Amphiboles of the International Mineralogical Association, commission on new minerals and mineral names. *Canad Mineral* 35:219–246
- Lemennicier Y (1996) Le complexe métamorphique du Sud Karakorum dans le secteur du Chogo Lungma (Baltistan-NE Pakistan). Etude structurale, métamorphique, géochimique et radiochronologique. *Géologie Alpine, Mémoire Hors Série* 26, LGCA Grenoble
- Lemennicier Y, Le Fort P, Lombardo B, Pêcher A, Rolfo F (1996) Tectonometamorphic evolution of the central Karakorum (Baltistan - northern Pakistan). *Tectonophysics* 260:119–143
- Letargo CMR, Lamb WM, Park JS (1995) Comparison of calcite + dolomite thermometry and carbonate + silicate equilibria: constraints on the conditions of metamorphism of the Llano uplift, central Texas, U.S.A. *Am Mineral* 80:131–143
- Mahéo G, Guillot S, Blichert-Toft J, Rolland Y, Pêcher A (2002) A slab breakout model for the Neogene thermal evolution of South Karakorum and South Tibet. *Earth Planet Sci Lett* 195:45–58
- Mahéo G, Bertrand H, Guillot S, Villa IM, Keller F, Capiez P (2004) The South Ladakh ophiolites (NW Himalaya, India): an intra-oceanic tholeiitic arc origin with implication for the closure of the Neo-Tethys. *Chem Geol* 203:273–303
- Massone HJ, Schreyer W (1987) Phengite geobarometry based on the limiting assemblage with K-feldspar, phlogopite and quartz. *Contrib Mineral Petrol* 96:212–224
- Morse JW, MacKenzie FT (1990) Geochemistry of sedimentary carbonates. *Developments in Sedimentology* 48, Elsevier, Amsterdam, pp 1–705
- Ogasawara Y, Zhang RY, Liou JG (1998) Petrogenesis of dolomitic marbles from Rongcheng in the Su-Lu ultrahigh-pressure metamorphic terrane, eastern China. *The Island Arc* 7:82–97
- Parkinson IJ, Arculus RJ (1999) The redox state of subduction zones: insights from arc-peridotites. *Chem Geol* 160:409–423
- Patriat P, Achache J (1984) India-Eurasia collision and chronology as implications for crustal shortening and driving mechanisms of plates. *Nature* 311:615–621
- Puhan D (1976) Metamorphic temperature determined by means of the dolomite-calcite solvus geothermometer. Examples from the central Damara Orogen (South West Africa). *Contrib Mineral Petrol* 58:23–28
- Rolland Y (2000) De la convergence intra-océanique à l'évolution post-collisionnelle: exemple de la convergence indo-asiatique en Himalaya du NW, du Crétacé à nos jours. PhD Thesis, Grenoble University
- Rolland Y (2002) From intra-oceanic convergence to post-collisional evolution: example of the India-Asia convergence in NW Himalaya, from Cretaceous to present. In: Rosenbaum G, Lister GS (eds) Reconstruction of the evolution of the Alpine-Himalayan orogeny. *J Virtual Explor* 8:183–205
- Rolland Y, Pêcher A, Picard C (2000) Middle Cretaceous back-arc formation and arc evolution along the Asian margin: the Shyok Suture Zone in northern Ladakh (NW Himalaya). *Tectonophysics* 325:145–173
- Rolland Y, Mahéo G, Guillot S, Pêcher A (2001) Tectono-metamorphic evolution of the Karakorum Metamorphic Complex (Dassu-Askole area, NE Pakistan): exhumation of mid-crustal HT-MP gneisses in a convergent context. *J Metamorph Geol* 19:717–737
- Rolland Y, Picard C, Pêcher A, Lapierre H, Bosch D, Keller F (2002a) The Ladakh Arc of NW Himalaya - Slab melting and melt-mantle interaction during fast northward drift of Indian Plate. *Chem Geol* 182:139–178
- Rolland Y, Picard C, Pêcher A, Carrio E, Sheppard SMF, Villa I, Oddone M (2002b) Presence and geodynamic significance of Cambro-Ordovician series in the SE Karakorum (N Pakistan). *Geodin Acta* 15:1–22
- Rolland Y, Villa IM, Guillot S, Mahéo G, Pêcher A (2005) Evidence for pre-Himalayan history and partial Mio-Pliocene re-equilibration in the Karakorum Crust (NW Himalaya) from  $^{40}\text{Ar}\text{-}^{39}\text{Ar}$  amphibole dating. *J Asian Earth Sci*
- Rowe KJ, Rutter EH (1990) Paleostress estimation using calcite twinning: experimental calibration and application to nature. *J Struct Geol* 12:1–18
- Rowley DR (1996) Age of initiation of collision between India and Asia: a review of stratigraphic data. *Earth Planet Sci Lett* 145:1–13
- Satish-Kumar M, Santosh M, Harley SL, Yoshida M (1996) Calc-silicate assemblages from the Kerala Khondalite Belt, South India: implications for pressure-temperature-fluid histories. *J Southeast Asian Earth Sci* 14:245–263
- Searle MP, Rex AJ, Tirrul R, Rex DC, Barnicoat A, Windley BF (1989) Metamorphic, magmatic and tectonic evolution of the central Karakorum in the Biafo-Baltoro-Hushe regions of northern Pakistan. *Geol Soc Am Spec Paper* 232:47–74

- Sheppard SMF, Schwarcz HP (1970) Fractionation of carbon and oxygen isotopes and magnesium between coexisting metamorphic calcite and dolomite. *Contrib Mineral Petrol* 26:161–198
- de Sigoyer J, Chavagnac V, Blichet-Toft J, Villa I, Luais B, Guillot S, Cosca M, Mascle G (2000) Dating the Indian continental subduction and collisional thickening in the northwest Himalaya: multichronology of the Tso Moriri eclogites. *Geology* 28:487–490
- Smith HA (1993) Characterization and timing of metamorphism within the Indo-Asian Suture Zone, Himalayas, Northern Pakistan. Unpublished PhD Thesis, Dartmouth College, New Hampshire, England
- Spalla MI, Lardeaux JM, Dal Piaz GV, Gosso G, Messiga B (1996) Tectonic significance of Alpine eclogites. *J Geodyn* 21(3):257–285
- Suzuki K (1977) Local equilibrium during the contact metamorphism of siliceous dolomites in Kasura-Mura, Gifu-ken, Japan. *Contrib Mineral Petrol* 61:79–89
- Tapponnier P, Peltzer G, Armijo R (1986) On the mechanics of the collision between Asia and India. In: Coward MP, Ries AC (eds) *Collision tectonics*. Geological Society, London, Special Publications 19:115–157
- Trommsdorff V (1972) Change in T-X during metamorphism of siliceous dolomitic rocks of the central Alps. *Schweiz Mineralogische Petrographische Mitteilungen* 52:567–571
- Veizer J, Davin A, Azmy K, Bruckschen P, Buhl D, Bruhn F, Carden G, Diener A, Ebner S, Godderis Y, Jasper T, Korte C, Pawellek F, Podlaha OG, Strauss H (1999)  $^{87}\text{Sr}/^{86}\text{Sr}$ ,  $\delta^{13}\text{C}$  and  $\delta^{18}\text{O}$  evolution of Phanerozoic seawater. *Chem Geol* 161:59–88
- Vernon RH (1981) Optical microstructure of partly recrystallised calcite in some naturally deformed marbles. *Tectonophysics* 78:601–612
- Vidal O, Parra T (2000) Exhumation paths of high pressure metapelites obtained from local equilibria for chlorite-phengite assemblages. *Geol J* 35(3/4):139–161
- Vidal O, Parra T, Trotet F (2001) A thermodynamic model for Fe-Mg aluminous chlorite using data from phase equilibrium experiments and natural pelitic assemblages in the 100–600°C, 1–25 kbar P-T range. *Am J Sci* 301:557–592
- Villa IM, Lemennicier Y, Le Fort P (1996) Late Miocene to Early Pliocene tectonometamorphism and cooling in south-central Karakorum and Indus-Tsangpo suture, Chogo Lungma area (NE Pakistan). *Tectonophysics* 260:201–214
- Wells PRA (1977) Pyroxene thermometry in simple and complex systems. *Contrib Mineral Petrol* 62:129–139
- White RW, Powell R (2002) Melt loss and the preservation of granulite facies assemblages. *J Metamorph Geol* 20:621–632
- Zeitler PK, Chamberlain CP, Smith H (1993) Synchronous anatexis, metamorphism, and rapid denudation at Nanga Parbat, Pakistan Himalaya. *Geology* 21:347–350